© 2026. Published by The Company of Biologists | Journal of Cell Science (2026) 139, jcs265013. doi:10.1242/jcs.265013

SHORT REPORT

BRD8 deficiency leads to progressive impairment of spermatogenesis in mice

Saya Nakagawa[1], Manabu Ozawa[2,3], Teh-Wei Wang[4,5], Tsuneo Ikenoue[1], Yumiko Isobe[1], Eigo Shimizu[6], Makoto Nakanishi[4], Seiya Imoto[6], Yoichi Furukawa[1,*] and Kiyoshi Yamaguchi[1,*]

ABSTRACT

BRD8, a member of the bromodomain-containing protein family, is a chromatin-associated protein that recognizes acetylated histones and recruits regulatory factors to modulate gene expression. Despite extensive studies of BRD8 in tumor biology, its physiological roles in normal tissues remain largely unknown. Given its enriched expression in the testis, we investigated the role of *Brd8* in male reproduction using a germ-cell-specific *Brd8* knockout mouse model. *Brd8* deficiency resulted in a marked reduction in testicular size and sperm count, accompanied by severe defects in germ-cell differentiation. Immunofluorescence staining for germ-cell markers demonstrated progressive spermatogenic defects, with a reduction in spermatids followed by declines in spermatocytes and spermatogonia at later ages. Single-cell transcriptome analysis of *Brd8*-knockout testes revealed transcriptional alterations in spermatogonia and spermatocytes, including dysregulation of translation-related pathways and reduced expression of genes involved in meiotic progression. In addition, VEGF-related signaling within the endothelial compartment was reduced in *Brd8*-knockout testes, suggesting secondary remodeling of the testicular microenvironment associated with progressive germ-cell dysfunction. Our findings provide new insights into the role of BRD8, an epigenetic reader, in male fertility.

KEY WORDS: Bromodomain-containing protein, Spermatogenesis, Germ cell differentiation, Mouse

INTRODUCTION

The bromodomain is a conserved four-helix bundle that specifically recognizes acetylated lysine residues. Bromodomain-containing proteins play essential roles in chromatin remodeling and transcriptional regulation through interactions with chromatin modifiers and remodelers (Filippakopoulos and Knapp, 2014). Consistent with these functions, bromodomain-containing proteins contribute to physiological homeostasis, and their dysregulation is associated with various human diseases, including cancer (Fujisawa and Filippakopoulos, 2017).

Bromodomain-containing protein 8 (BRD8) was initially characterized as a skeletal muscle-abundant protein (Nielsen et al., 1996) and as a co-activating protein of thyroid hormone receptor (Monden et al., 1997). Subsequent studies identified BRD8 as a subunit of the TIP60 acetyltransferase complex, a multiprotein complex that regulates chromatin structure and gene transcription through histone acetylation (Cai et al., 2003). Through its bromodomain, BRD8 is thought to recognize acetylated histones and contribute to the recruitment or stabilization of the TIP60 complex at target chromatin regions, thereby facilitating transcriptional regulation. Therefore, deregulated expression of BRD8 observed in colorectal cancer (Yamaguchi et al., 2023, 2010), breast cancer (Yu et al., 2023) and glioblastoma (Sun et al., 2023) leads to transcriptional abnormalities, resulting in a malignant phenotype characterized by increased cell proliferation, inhibition of apoptosis, enhanced epithelial-mesenchymal transition and reduced sensitivity to chemotherapy (Yamaguchi et al., 2024). To date, BRD8 has been extensively studied in the context of tumor biology, but its physiological roles in normal tissues remain poorly understood.

Spermatogenesis is one of the most extensive chromatin remodeling processes in mammals. During germ-cell differentiation, the genome undergoes large-scale transcriptional reprogramming and histone hyperacetylation (Govin et al., 2004). Eventually, histones are replaced by transition proteins and protamine. Disruption of chromatin remodeling factors often leads to impaired germ-cell maturation and infertility (Li et al., 2014; Matzuk et al., 2012; Wang et al., 2022). Thus, together with our previous observation of enriched BRD8 expression in the testis (Yamaguchi et al., 2023), these findings suggest that epigenetic reader BRD8 may contribute to male germ-cell differentiation.

In this study, we demonstrate that BRD8 is essential for spermatogenesis and male fertility. Using a germ-cell-specific *Brd8* knockout mouse model, we show here that *Brd8* deficiency disrupts germ cell differentiation and prevents the production of mature spermatozoa. These findings highlight a crucial role for BRD8 acetyl-lysine reader in germ-cell maturation.

RESULTS AND DISCUSSION

Expression of *Brd8* and its long-form isoform in the testis

There are two major forms of human BRD8 that differ in their bromodomain (BD) composition. Isoform 1 and related variants contain only BD1, while isoform 2, referred to as the ‘long form’,

[1]Division of Clinical Genome Research, Advanced Clinical Research Center, The Institute of Medical Science, The University of Tokyo, Tokyo 108-8639, Japan. [2]Core Laboratory for Developing Advanced Animal Models, Center for Experimental Medicine and Systems Biology, The Institute of Medical Science, The University of Tokyo, Tokyo 108-8639, Japan. [3]Laboratory of Reproductive Systems Biology, Center for Experimental Medicine and Systems Biology, The Institute of Medical Science, The University of Tokyo, Tokyo 108-8639, Japan. [4]Division of Cancer Cell Biology, The Institute of Medical Science, The University of Tokyo, Tokyo 108-8639, Japan. [5]Project Division of Generative AI Utilization Aging Cells, The Institute of Medical Science, The University of Tokyo, Tokyo 108-8639, Japan. [6]Division of Health Medical Intelligence, Human Genome Center, The Institute of Medical Science, The University of Tokyo, Tokyo 108-8639, Japan.

*Authors for correspondence (yofurukawa@g.ecc.u-tokyo.ac.jp; kiyamagu@g.ecc.u-tokyo.ac.jp)

S.N., 0000-0002-5893-1663; M.O., 0000-0003-3284-7161; M.N., 0000-0002-6707-3584; S.I., 0000-0002-2989-308X; Y.F., 0000-0003-0462-8631; K.Y., 0000-0003-2113-4369

This is an Open Access article distributed under the terms of the Creative Commons Attribution License (https://creativecommons.org/licenses/by/4.0), which permits unrestricted use, distribution and reproduction in any medium provided that the original work is properly attributed.

Handling Editor: Guangshuo Ou
Received 1 May 2026; Accepted 21 September 2026

Journal of Cell Science (2026) 139, jcs265013. doi:10.1242/jcs.265013

contains BD1 and an additional C-terminal bromodomain (BD2) (Fig. S1A). Of these, the human *BRD8* long-form isoform is exclusively expressed in the testis (GTEx Portal; https://gtexportal.org/home/) (Fig. 1A). Unlike human *BRD8*, mouse *Brd8* lacks the long-form isoform, according to the NCBI database. Instead, the mouse genome encodes *Brd8dc*, which contains BD2 alone (Fig. S1A). To determine whether the long-form isoform is expressed in mice, we performed RT-PCR using mouse testis cDNA with primers spanning the 5′-UTR of *Brd8* and the 3′-UTR of *Brd8dc* (Fig. S1A). The amplified products were purified and subjected to long-read sequencing. As a result, we identified a previously unannotated transcript that encodes a long-form isoform containing both BD1 and BD2 (long form 1), analogous to human isoform 2 (Fig. S1B). This analysis also uncovered two additional major long-form variants of *Brd8* (long forms 2 and 3) and novel splice junctions in the mouse testis (Table S1). We further analyzed the transcription start sites (TSSs) and promoter activity at the *Brd8* locus using the CAGE (Cap Analysis of Gene Expression) database (FANTOM5 SSTAR; https://fantom.gsc.riken.jp/5/sstar/Main_Page). As shown in Fig. 1B, a CAGE peak was detected at the *Brd8* TSS, but not at the *Brd8dc* TSS, in the mouse testis, indicating that *Brd8* and its long-form isoforms are the predominant transcripts expressed in this tissue. We next confirmed the presence of BRD8 protein corresponding to the long-form isoforms in mouse testis (Fig. 1C). In addition, immunohistochemistry revealed predominant BRD8 expression in germ cells of the mouse testis (Fig. 1D). Together, these findings support a testis-specific role for BRD8 and provided the basis for the subsequent *Brd8* knockout strategy.

BRD8 plays a crucial role in male fertility

To elucidate the biological role of BRD8 in the testis, we generated *Brd8* floxed mice by CRISPR/Cas9-mediated genome editing of V6.5 (B6J/129) embryonic stem (ES) cells. LoxP sites were inserted into introns 16 and 19 of *Brd8* to enable Cre-mediated excision of a genomic region encoding most of BD1. Deletion of this region was also expected to cause a frameshift, leading to a premature stop codon and disruption of the downstream coding sequence, including BD2 (Fig. 2A; Fig. S2A). Founder males derived from genome-edited ES cells were crossed with C57BL/6J females, and germline transmission of the floxed allele was confirmed by PCR genotyping of genomic DNA (Fig. S2B). We then crossed *Brd8* floxed mice with *Nanos3-Cre* transgenic mice to generate germ-cell-specific *Brd8* knockout mice (*Nanos3-Cre; Brd8*$^{flox/flox}$). Nanos3-Cre-mediated recombination has been reported to increase after

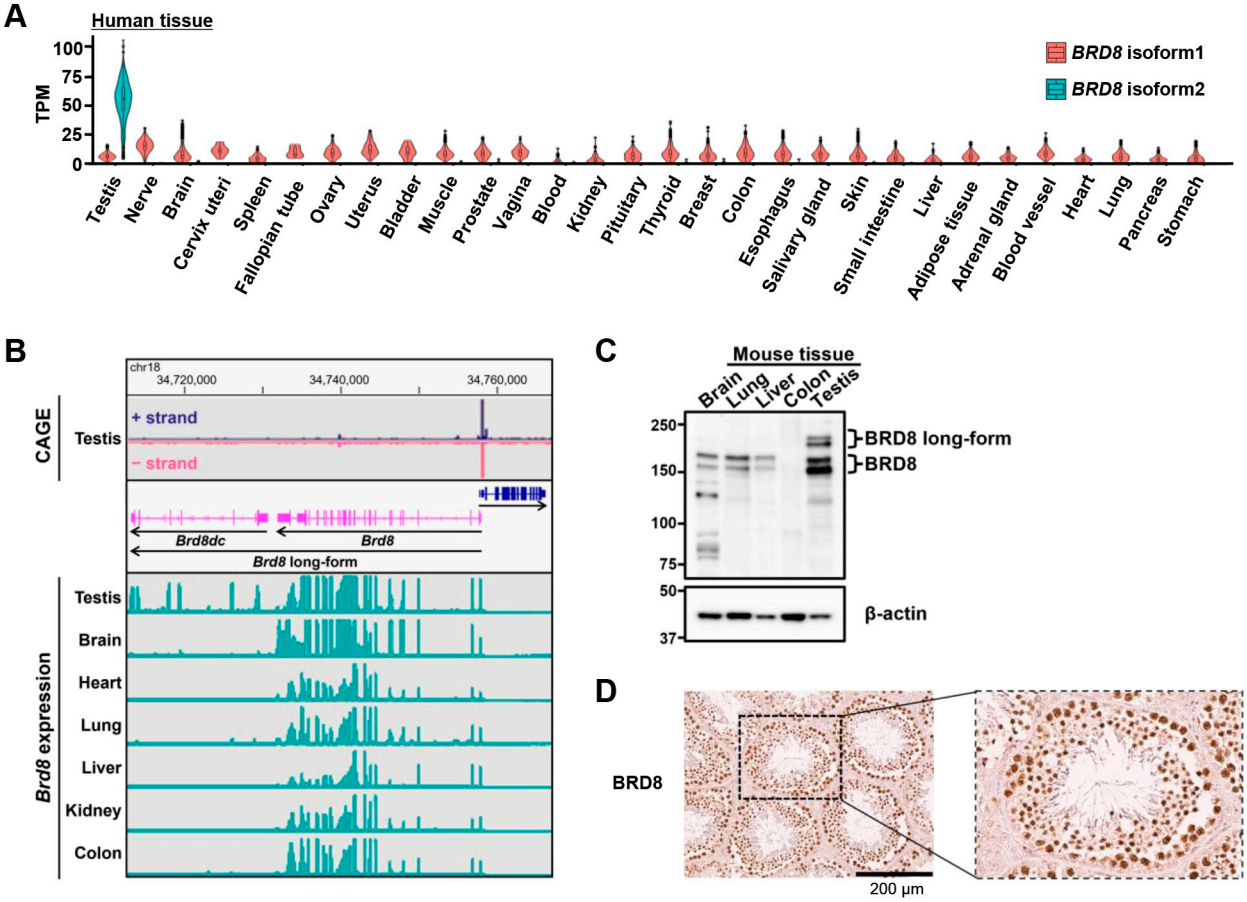


Fig. 1. Expression of BRD8 isoforms in mouse testis. (A) Violin plots showing the expression levels of *BRD8* transcripts across human tissues. Boxes and whiskers within the violin plot denote the median (line), interquartile range (box) and the minimum and maximum values within 1.5× the interquartile range (whiskers). Transcripts per million (TPM) data were downloaded from https://gtexportal.org/home/downloads/adult-gtex/bulk_tissue_expression#bulk_tissue_expression-gtex_analysis_v8-rna-seq. (B) Characterization of transcriptional profiles at the *Brd8* and *Brd8dc* loci (GRCm39). Strand-specific TSS activity was obtained from CAGE data (mouse testis). RNA-seq coverage tracks were generated from ENCODE data (https://www.encodeproject.org/) using the following datasets: testis, ENCFF960KND; brain, ENCFF277JND; heart, ENCFF105PMT; lung, ENCFF663ZDA; liver, ENCFF261RMC; kidney, ENCFF983LLT; colon, ENCFF858AGA. (C) Immunoblotting of BRD8 in mouse tissues. β-actin was used as a loading control. Approximate molecular weights are shown in kDa on the left. Blots shown are representative of two experiments. (D) Immunohistochemical staining of BRD8 in a mouse testis section. Images shown are representative of two samples.

Journal of Cell Science (2026) 139, jcs265013. doi:10.1242/jcs.265013

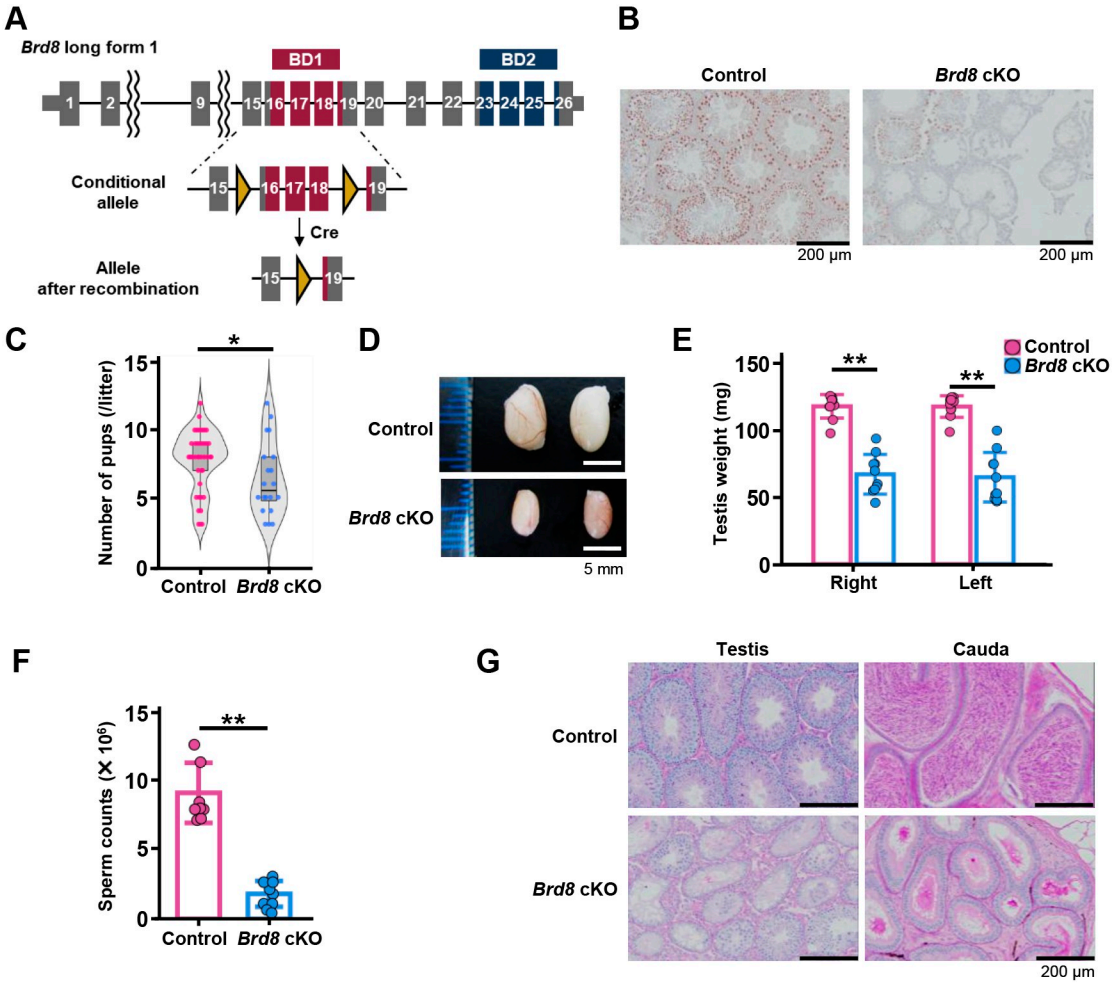


Fig. 2. Phenotypic characterization of germ cell-specific *Brd8* conditional knockout mice. (A) Schematic of the *Brd8* conditional allele and Cre-mediated recombination strategy. LoxP sites (yellow triangles) were inserted into intron 16 and intron 19 to flank the exons encoding the first bromodomain (BD1). Cre-mediated recombination excises these exons, resulting in a frameshift and premature termination of translation. (B) Representative histological images of BRD8 staining in testis sections from control and *Brd8* cKO mice. Images are representative of two samples. (C) Comparison of litter size. Boxes and whiskers within the violin plot denote the median (line), interquartile range (box) and the minimum and maximum values within 1.5× the interquartile range (whiskers). Statistical significance was determined by unpaired, two-tailed *t*-test. Each dot represents one litter. A total of 41 litters (Control) and 20 litters (*Brd8* cKO) were obtained from 10 males per group mated with 15 females per group. **P*<0.05. See also Fig. S3A. (D) Representative testicular morphology in control and *Brd8* cKO mice. Images are representative of 10 samples. (E) Left and right testicular weights in control and *Brd8* cKO mice (*n*=10 per group). Data are presented as mean±s.d. Statistical significance was determined by unpaired, two-tailed *t*-test. ***P*<0.01 versus control mice. (F) Sperm counts in the cauda epididymis (*n*=10 per group). Data are presented as mean±s.d. Statistical significance was determined by unpaired, two-tailed *t*-test. ***P*<0.01 versus control mice. (G) PAS staining of testicular sections and Hematoxylin staining of cauda epididymal sections from control and *Brd8* cKO mice. Images are representative of two samples.

embryonic day (E)13.5 (Inoue et al., 2022) and to become highly efficient by the early postnatal stage (Zhou et al., 2017). In this model, BRD8 expression was markedly reduced in germ cells of the knockout mice, although the extent of BRD8 loss varied among seminiferous tubules (Fig. 2B; Fig. S5A).

To assess male fertility, *Nanos3-Cre; Brd8*$^{+/+}$ (control) or *Nanos3-Cre; Brd8*$^{flox/flox}$ (*Brd8* cKO) males (*n*=10 per genotype) were individually paired with one or two wild-type females for 3 months. Females mated with control males produced a total of 41 litters, whereas those mated with *Brd8* cKO males produced only 20 litters, likely due to reduced fertility, as reflected by fewer pups per litter (Fig. 2C; Fig. S3A). These results suggested that *Brd8* affects male reproductive function.

We also attempted to generate a whole-body *Brd8* knockout model by crossing *Brd8* floxed mice with *CAG-Cre* transgenic mice, which produced *Brd8*$^{+/-}$ offspring. However, subsequent intercrosses failed to generate homozygous knockout mice (Fig. S3B).

Testicular morphology and spermatogenesis in *Brd8* cKO mice

To investigate the cause of impaired fertility, we analyzed the reproductive tracts of *Brd8* cKO males. The knockout significantly reduced testis size (control: right, 9.1±0.74 mm; left, 9.0±0.67 mm; cKO: right, 7.2±0.63 mm; left, 7.2±0.63 mm; mean±s.d.) and weight (control: right, 118.2±8.82 mg; left, 118.0±8.07 mg; cKO: right, 67.3 ±14.87 mg; left, 65.1±18.53 mg; mean±s.d.) (Fig. 2D,E), with a slight reduction in body weight (Fig. S3C). Sperm counts in *Brd8* cKO mice were significantly lower than those in control mice (Fig. 2F). Additionally, Periodic acid–Schiff (PAS) staining revealed morphological abnormalities, including disorganized seminiferous tubules, reduced germ-cell layers and decreased sperm accumulation

Journal of Cell Science (2026) 139, jcs265013. doi:10.1242/jcs.265013

in the cauda epididymis (Fig. 2G). Collectively, these findings indicate impaired spermatogenesis in *Brd8* cKO mice.

Age-dependent impairment of spermatogenesis in *Brd8* cKO testes

To determine how *Brd8* cKO affects spermatogenesis, we performed immunofluorescence staining using stage-specific germ-cell markers. Testis sections from control and *Brd8* cKO mice were analyzed at multiple developmental stages, including postnatal day (P) 0, P5, P21, P35, 8 weeks and 18 weeks of age. To assess germ-cell differentiation at different ages, PLZF (also known as ZBTB16), SYCP3 and TRA54 were used as markers of spermatogonia, spermatocytes and spermatids, respectively. During the first wave of spermatogenesis, PLZF-positive spermatogonia and SYCP3-positive spermatocytes were largely preserved in *Brd8* cKO testes, whereas TRA54-positive spermatids were already reduced at P35 (Fig. 3A,B; Fig. S4C). At 8 weeks of age, SYCP3-positive spermatocytes were significantly reduced, together with a decreasing trend in PLZF-positive spermatogonia. By 18 weeks, both SYCP3-positive spermatocytes and PLZF-positive spermatogonia were

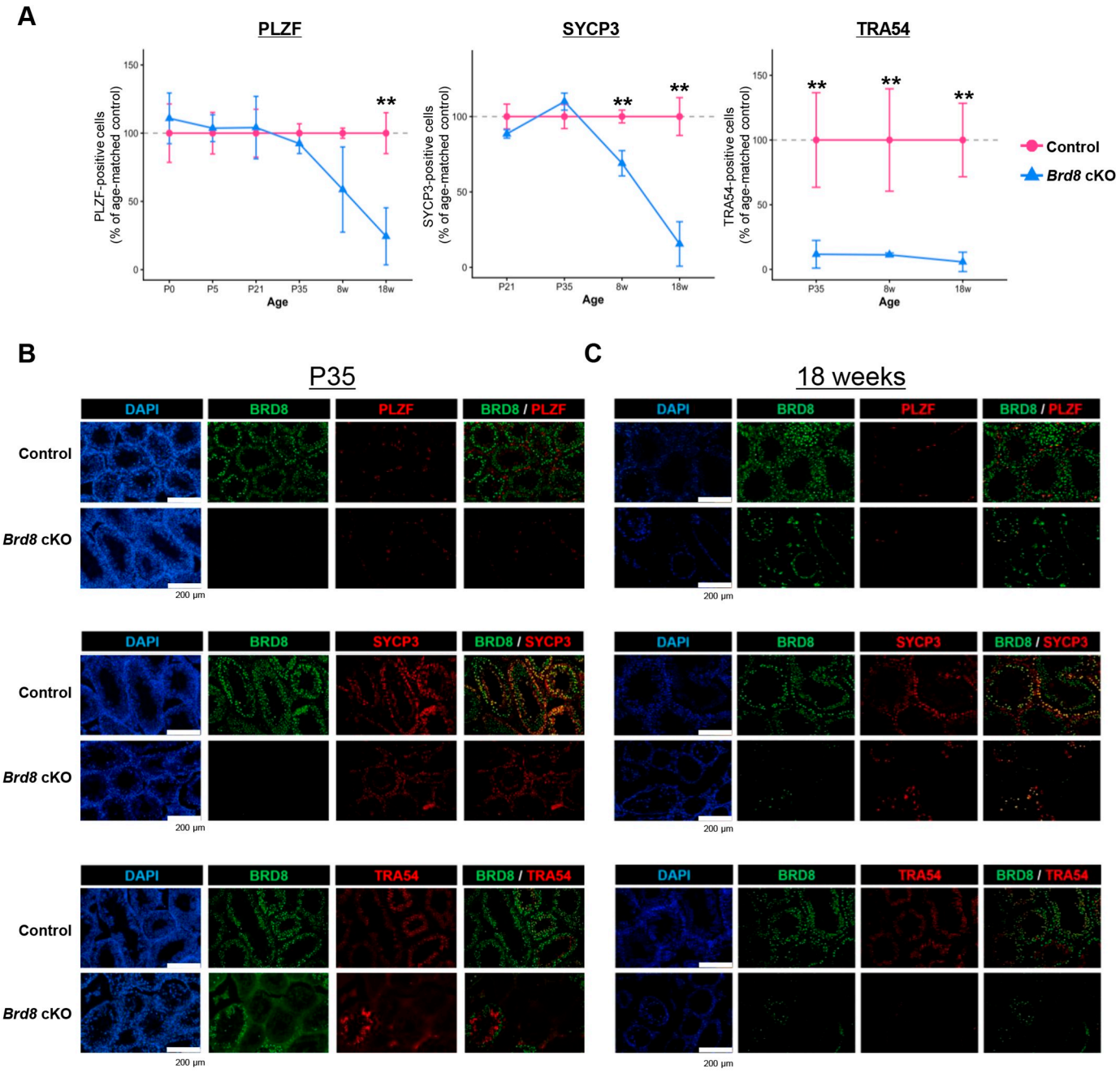


Fig. 3. *Brd8* deficiency causes progressive germ-cell defects. (A) Quantification of PLZF-positive spermatogonia, SYCP3-positive spermatocytes and TRA54-positive spermatids in control and *Brd8* cKO testes at the indicated postnatal ages. Values are expressed relative to the mean value of the control group at each age, which was set to 100%. Data are presented as mean±s.d. (n=3). Statistical significance was determined by unpaired, two-tailed t-test. **P<0.01 versus control mice. (B,C) Representative immunofluorescence images of testicular sections from control and *Brd8* cKO mice at P35 (B) and 18 weeks of age (C). Sections were stained for BRD8 together with PLZF, a marker of spermatogonia; SYCP3, a marker of spermatocytes; or TRA54, a marker of spermatids. DAPI was used to visualize nuclei. Images are representative of three samples.

markedly reduced (Fig. 3A,C; Fig. S4A,B). These findings suggest a progressive spermatogenic phenotype characterized by an initial reduction in spermatids, followed by declines in spermatocytes and spermatogonia at later ages.

Cellular heterogeneity and transcriptional differences in control and *Brd8* cKO testes

Given the role of BRD8 in transcriptional activation, we performed single-cell RNA sequencing (scRNA-seq) using two independent control–cKO pairs to characterize cell-type-specific transcriptional changes in *Brd8* cKO testes. Because BRD8 depletion efficiency differed between the two cKO mice (Fig. S5A), the results of downstream analyses, including cell-type annotation and cell–cell communication analysis, were presented separately for each control–cKO pair (Fig. 4; Fig. S5). In both pairs, cells from control and *Brd8* cKO mice were grouped into 21 clusters and assigned to ten cell types based on canonical marker genes (Fig. 4A; Fig. S5B,C). Pseudotime analysis revealed a continuous trajectory from spermatogonia to elongating spermatids, consistent with the expected progression of germ-cell differentiation (Fig. 4B). Analysis of cellular composition revealed a marked reduction in elongating spermatids in *Brd8* cKO testes in both pairs (Fig. 4C; Fig. S5D). The apparent relative increase in spermatogonia and spermatocytes likely reflected the depletion of elongating spermatids rather than an actual expansion of these earlier germ-cell populations, consistent with the immunofluorescence analyses (Fig. 3A; Table S2).

To investigate the potential role of *Brd8* in germ-cell differentiation, we analyzed its expression across cell types. *Brd8* was highly expressed in spermatogonia and spermatocytes (Fig. 4D). Despite its predominant expression in early germ cells, the reduction of elongating spermatids in *Brd8* cKO testes suggests that *Brd8* is required for proper differentiation during spermatogenesis.

To characterize transcriptional alterations associated with *Brd8* deficiency, we first compared gene expression changes in spermatogonia and spermatocytes between control and cKO testes for each experimental pair. Comparison of the overall patterns of gene expression changes between the two independent control–cKO pairs showed broad concordance (Fig. S5E). We therefore merged the two datasets and performed differential expression analysis in spermatogonia and spermatocytes to identify robust *Brd8*-associated transcriptional changes. This analysis identified 155 genes significantly downregulated in spermatogonia and 583 genes in spermatocytes (Fig. 4E,F; Tables S3 and S4). Of note, gene ontology (GO) analysis of the downregulated genes showed prominent enrichment of translation-related processes in both spermatogonia and spermatocytes (Fig. 4E,F; Tables S5 and S6). Translational regulation has been shown to play an important role at multiple stages of spermatogenesis, including spermatogonial differentiation and meiotic progression (Busada et al., 2015; Fang et al., 2025; Sun et al., 2010). In addition, several genes implicated in germ-cell development were downregulated in *Brd8*-deficient spermatocytes, including *Sycp3* and *Syce3*, which encode components of the synaptonemal complex, and *Tdrd7*, a chromatoid body factor. Proper synaptonemal complex assembly is essential for homologous chromosome synapsis and meiotic progression (Yuan et al., 2000), while TDRD7 is required for chromatoid-body organization and ribonucleoprotein (RNP) remodeling during spermatid development (Shang et al., 2007; Tanaka et al., 2011). Together, these findings suggest that *Brd8* supports germ-cell development by regulating translation-related transcriptional programs in spermatogonia and spermatocytes and genes associated with meiotic progression in spermatocytes. Collectively, these transcriptional changes provide insight into the molecular mechanisms through which *Brd8* contributes to spermatogenesis.

Despite the fact that *Brd8* deletion was restricted to germ cells, gene expression changes were also observed in somatic-cell populations, with 646 and 199 differentially expressed genes detected in Sertoli and Leydig cells, respectively (Fig. S6A; Tables S7 and S8). These changes may represent secondary consequences of germ-cell dysfunction rather than direct effects of *Brd8* deficiency. Indeed, germ-cell depletion has been shown to alter the gene expression profiles of Sertoli cells (Gewiss et al., 2021), suggesting that germ-cell dysfunction may alter interactions between germ cells and surrounding somatic cells, thereby affecting the local microenvironment within the seminiferous tubules. In line with these transcriptional changes, CellChat analysis identified changes in the intercellular communication network between control and *Brd8* cKO testes (Fig. S6B). In particular, VEGF-related signaling was reduced in both independent comparisons and was predominantly associated with endothelial-to-endothelial communication (Fig. 4G-I; Tables S9-S11). Because testicular endothelial cells contribute to the spermatogonial stem-cell niche and support spermatogenesis (Bhang et al., 2018), the altered VEGF-related signaling may be relevant to the spermatogenic phenotype. Alternatively, it may reflect secondary remodeling of the testicular microenvironment associated with severe spermatogenic failure, germ-cell apoptosis or germ-cell loss. Whether this alteration contributes to the progression of the spermatogenic phenotype remains to be determined in future studies.

In our previous study, we found that BRD8 regulates DNA replication and cell cycle progression via pre-replicative complex components, including ORC and MCM family genes, in colorectal cancer cells (Yamaguchi et al., 2023); however, these genes were not altered in *Brd8* cKO testes. BRD8 regulates transcription through interactions with chromatin modifiers, remodelers and associated co-factors, suggesting that its target genes are determined in a context-dependent manner. Of particular interest, the testis-expressed BRD8 long-form isoform contains an additional BD2 compared with the major BRD8 isoform 1 expressed in other tissues (Fig. 1A), suggesting that it may contribute to tissue-specific transcriptional regulation. Studies of BET (bromodomain and extraterminal domain) proteins have demonstrated distinct roles for their tandem bromodomains, BD1 and BD2 (Gilan et al., 2020; Miller et al., 2016). Selective inhibition studies of the BET proteins have shown that BD1 is primarily required for steady-state gene expression, whereas BD2 is particularly important for rapid transcriptional responses to inflammatory stimuli (Gilan et al., 2020). In contrast to BET proteins, the functional differences between BRD8 BD1 and BD2 remain poorly understood. The development of BRD8 inhibitors with selectivity for BD1 or BD2 could help elucidate the testis-specific role of BD2. Further characterization of isoform- and bromodomain-specific BRD8 functions will be important for understanding how BRD8 regulates testis-specific transcriptional programs during spermatogenesis.

MATERIALS AND METHODS

Animals

C57BL/6J female mice used for fertility tests were obtained from CLEA Japan. *Nanos3-Cre* mice were kindly provided by Dr Yumiko Saga (National Institute of Genetics, Japan) (Suzuki et al., 2008). The mice were maintained under pathogen-free conditions in a 12-h light/dark cycle, with

Journal of Cell Science (2026) 139, jcs265013. doi:10.1242/jcs.265013

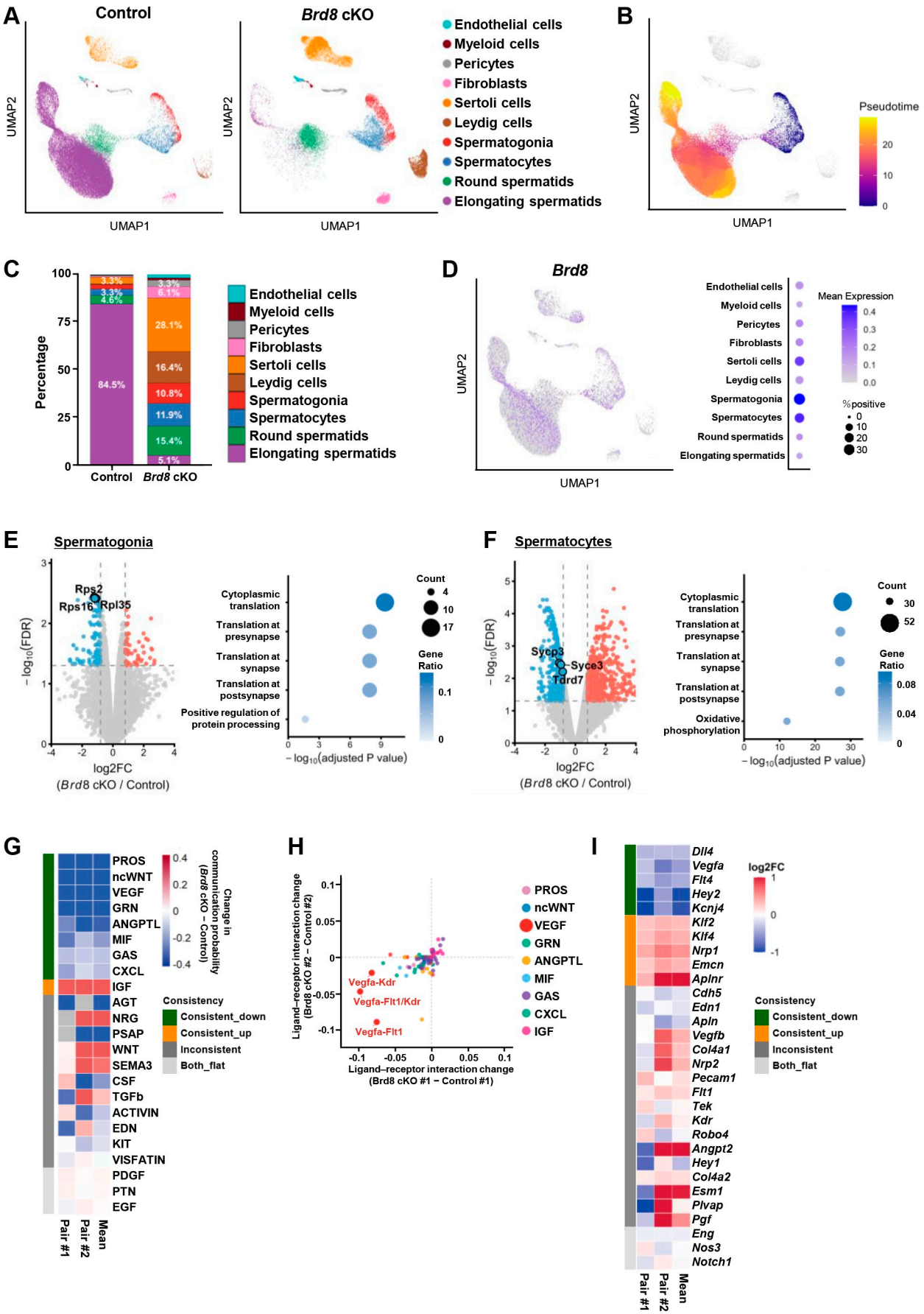


Fig. 4. See next page for legend.

Journal of Cell Science

Fig. 4. Single-cell analysis reveals impaired spermiogenesis in *Brd8*-deficient mouse testes. (A) UMAP visualization of scRNA-seq data from control and *Brd8* cKO testes (*n*=2), colored by cell type using canonical marker genes. (B) Pseudotime trajectory analysis of germ cells. Pseudotime values indicate the relative position of cells along the inferred differentiation trajectory, with lower and higher values representing earlier and later states, respectively. (C) Cell-type composition in control and *Brd8* cKO testes. (D) *Brd8* expression across cell types in the mouse testis. In the dot plot (right), dot size and color intensity represent the percentage of expressing cells and the average expression level, respectively. (E,F) Volcano plots and GO enrichment analyses of differentially expressed genes in spermatogonia (E) and spermatocytes (F). The five most significantly enriched GO terms are shown. Genes with an FDR *q*-value<0.05 and $|\log_2 FC| \geq 0.8$ were considered significantly differentially expressed. (G) Heatmap showing changes in communication probability between control and *Brd8* cKO testes across signaling pathways from two independent comparisons. (H) Comparison of CellChat-inferred ligand–receptor interaction changes between the two independent control–*Brd8* cKO comparisons. Each dot represents a ligand–receptor interaction and is colored according to the corresponding signaling pathway. VEGFA–FLT1, VEGFA–KDR and VEGFA–FLT1/KDR interactions were concordantly decreased in both comparisons. (I) Altered expression of VEGF-related genes in endothelial cells (control versus *Brd8* cKO). Columns indicate the $\log_2$ fold changes ($\log_2$FC) for Pair #1 and Pair #2, as well as the mean $\log_2$FC across the two comparisons. Pair #1 was used for cell clustering (A), pseudotime analysis (B), cell-type annotation (C) and *Brd8* expression analysis (D). The merged datasets from Pair #1 and Pair #2 were used for analyses of differentially expressed genes (E,F).

food and water provided *ad libitum* at the animal facility of the Institute of Medical Science, The University of Tokyo, Japan. All animal experiments were conducted with the approval of the Institutional Animal Care and Use Committee of The University of Tokyo (approval number: A2024IMS035), in accordance with their guidelines and the ARRIVE guidelines (https://arriveguidelines.org).

Generation of floxed mice

We designed targeting vectors containing loxP sites flanking exons 17-19, including the bromodomain of *Brd8*. Guide RNAs with the sequence of 5′-ATACAAGAGTGCTACTAAGT-3′ and 5′-TGGGCTTGACTCTAACGTCG-3′ were designed and used to target intron 16 and intron 19 of *Brd8*, respectively. The *Brd8 flox* ES cell lines were generated as previously described (Ozawa et al., 2022). Briefly, targeting vectors were constructed by cloning synthesized *Brd8 flox* sequences into pUC vectors (Azenta Life Sciences). The targeting vector featured 1000-bp 5′ and 3′ homology arms to facilitate knock-in of the *Brd8* locus. For genome editing, 1.0×10^5 V6.5 ES cells (C57BL/6×129SvJae) were transfected with 1 µg of the targeting vector in 10 µl Cas9 RNP complexes using the Neon NxT Electroporation System 10 µl kit (Thermo Fisher Scientific). The RNP complex consisted of Alt-R Sp. Cas9 Nuclease V3 (0.3 µg/µl, Integrated DNA Technologies) and annealed gRNA (10 µM, Integrated DNA Technologies), supplemented with Electroporation Enhancer (21.6 µM, Integrated DNA Technologies). Electroporation was performed with two pulses at 1200 V for 20 ms. Post-electroporation, cells were cultured in 6-cm dishes and passaged once before colony picking. Correct targeting via homologous recombination was confirmed by PCR-based genotyping. Validated knock-in ES cell lines were injected into blastocysts from ICR mice (Japan SLC) to generate chimeric mice. Chimeric mice were crossed with C57BL/6J mice to obtain heterozygous floxed mice. These mice were subsequently backcrossed to C57BL/6J mice for ten generations. Genotyping of *Brd8* floxed mice was performed by PCR using primers flanking the loxP sites and GoTaq Master Mixes (Promega). The primer sequences used are listed in Table S12.

Fertility test

Male mice aged 2 months were individually housed with one or two 8-week-old females for 3 months. The number of pups after each delivery was recorded.

Counting the number of sperm cells

Spermatozoa from the cauda epididymis were suspended in DMEM (Thermo Fisher Scientific) containing 10% fetal bovine serum for 1 h at 37°C. The number of spermatozoa was counted with a hemocytometer.

Immunoblotting

Tissues were homogenized in radioimmunoprecipitation assay buffer (50 mM Tris-HCl, pH 8.0, 150 mM NaCl, 0.5% sodium deoxycholate, 1% Nonidet P-40, 0.1% sodium dodecyl sulphate) supplemented with a Protease Inhibitor Cocktail Set III (Merck). The proteins were separated by SDS-PAGE and transferred to a nitrocellulose membrane (Cytiva). After blocking with 5% skim milk powder in TBS-T (Tris-buffered saline with 0.1% Tween 20), the membranes were incubated with anti-BRD8 antibody (Active Motif, 61008, AB_2615053, 1:1000) or anti-β-actin antibody (Merck, A5441, AB_476744; 1:2500) overnight at 4°C. Horseradish peroxidase-conjugated anti-rabbit IgG (Cytiva, NA9340, AB_772191; 1:3000) or anti-mouse IgG (Cytiva, NA931, AB_772210; 1:3000) served as the secondary antibody. The membranes were incubated with ImmunoStar LD (Fujifilm Wako Pure Chemical) or SuperSignal West Pico Chemiluminescent Substrate (Thermo Fisher Scientific), and the chemiluminescence images were captured using an Amersham Imager 600 system (Cytiva). Full blot images are shown in Fig. S7.

PAS staining

Testes and epididymides were fixed using Bouin's fluid (Fujifilm Wako Pure Chemical). Subsequently, the tissues were embedded in paraffin-filled cassettes and sectioned. The sections were subjected to PAS staining (Sept.Sapie).

Immunohistochemistry

Testes were fixed in 4% formalin and embedded in paraffin. Tissue sections were deparaffinized in xylene and rehydrated through a graded ethanol series. Antigen retrieval was performed using 0.01 M citrate buffer (pH 6.0) with autoclave heating at 108°C for 10 min. Endogenous peroxidase activity was quenched by incubation in 0.3% hydrogen peroxide for 20 min. The sections were then blocked with 5% goat serum (Abcam, ab7481, AB_2716553) in TBS containing 0.05% Tween 20 for 30 min at room temperature. The sections were incubated overnight at 4°C with anti-BRD8 antibody (Sigma-Aldrich, HPA001841, AB_1845438; 1:1000) diluted in Can Get Signal Immunostain Solution A (Toyobo). After washing, the sections were incubated with an HRP-labeled secondary antibody using the EnVision+ System (Dako, K5007). Signals were visualized using 3,3′-diaminobenzidine substrate. The sections were counterstained with Hematoxylin, then dehydrated and mounted. Whole-slide images were acquired using a NanoZoomer S360MD slide scanner (Hamamatsu Photonics).

Immunofluorescence staining

Testes were fixed in a 4% formalin solution and embedded in paraffin. Tissue sections were deparaffinized with xylene and rehydrated in a graded series of ethanol. Antigen retrieval was performed using 0.01 M citrate buffer (pH 6.0) and autoclave heating at 108°C for 10 min. The slides were incubated with 5% goat serum (Abcam, ab7481, AB_2716553)/0.05% Tween 20/TBS for 30 min to block non-specific hybridization, followed by incubation with primary antibodies overnight at 4°C in a humidified chamber. Secondary antibodies were applied to visualize the signals. Samples were mounted with VECTASHIELD mounting medium containing DAPI (Vector Laboratories, H-1800) and examined using a confocal microscope (ECLIPSE Ti2, Nikon). Antibodies used for the staining are listed in Table S13.

Targeted long-read nanopore sequencing

cDNA from a mouse testis was used as a template for PCR amplification using KOD One with primers designed in the 5′-UTR of *Brd8* and the 3′-UTR of *Brd8dc* (Table S1). After purification, the PCR products were sequenced on the PromethION platform (Oxford Nanopore Technologies) using the Ligation Sequencing Kit V14 (Oxford Nanopore Technologies, SQK-LSK114). Sequencing reads were aligned to the mouse reference

genome (GRCm39) using minimap2 (v2.26) (Li, 2018). Reads containing primer sequences were extracted, and reads with hard-clipped alignments were removed. A total of 37,618 filtered reads were subjected to detection and quantification of the *Brd8* long-form isoforms using FLAIR (v2.0.0) (Tang et al., 2020). Additionally, RegTools (v1.0.0) was used to determine whether the long form of *Brd8* has a novel splice junction (Cotto et al., 2023). The filtered reads and gene annotation file (gencode.vM38.annotation.gtf) were also used for this analysis.

Analysis of CAGE data

A fastq file was downloaded from the CAGE database (mouse adult testis, 57-7G5, FANTOM5 SSTAR; https://fantom.gsc.riken.jp/5/sstar/Main_Page). Sequencing reads were aligned to the mouse reference genome (GRCm39) using STAR (v2.7.3a) (Dobin et al., 2013). The 5′-end positions were extracted from aligned reads using Samtools (v1.19) to identify TSSs (Li et al., 2009). Bedtools (v2.29.1) and bedGraphToBigWig (v2.8) were used to generate BigWig tracks for visualization of CAGE peaks in Integrative Genomics Viewer (Kent et al., 2010; Quinlan and Hall, 2010; Thorvaldsdóttir et al., 2013).

Isolation of testicular cells for scRNA-seq

Testes were dissected from two control and two cKO mice at 18 weeks of age. After removing the tunica albuginea, the tissues were digested in three steps. First, samples were incubated in 6 ml collagenase type I (120 U/ml in 1× DMEM) with 10 µl DNase I (1 mg/ml in 50% glycerol) at 37°C for 15 min. The seminiferous tubules were then isolated by sedimentation for 1 min at room temperature. Then, 4 ml collagenase type I, 50 µl trypsin (50 mg/ml in 1 mM HCl) and 10 µl DNase I were added and incubated at 37°C for 15 min, followed by gentle trituration for 3 min. Next, 30 µl trypsin and 150 µl DNase I were added, and the mixture was incubated at 37°C for 10 min. After quenching the reaction with 400 µl fetal bovine serum, the suspension was filtered twice through a 40-µm strainer and immediately processed for scRNA-seq library preparation.

scRNA-seq and data analysis

Isolated cells were processed with the Illumina single cell 3′ RNA Prep T10 Kit according to the manufacturer's instructions (Illumina). Libraries were sequenced on the DNBSEQ-G400RS platform (MGI Tech). The DRAGEN Single Cell RNA pipeline (v4.4.6000) was used to process cell barcodes and unique molecular identifiers and to align sequencing reads to the mouse reference genome (GRCm39). After obtaining the feature-barcode matrices, we utilized Seurat package (v5.3.0) (Hao et al., 2024) in R language (v4.2.1). Four samples (Control#1, Control#2, *Brd8* cKO#1, *Brd8* cKO#2) were merged, and genotype metadata were assigned. Cells were retained if they met the following criteria: 500<nFeature_RNA<4000, nCount_RNA<10,000 and percent.mt<5%. After initial clustering and cell-type annotation, potential ambient RNA contamination was estimated and corrected using DecontX (Yang et al., 2020). The DecontX-corrected count matrices were then used to reconstruct the Seurat object, followed by normalization, dimensionality reduction, UMAP visualization, and downstream analyses. Cell types were annotated by integrating the expression of canonical marker genes with cluster-enriched genes identified using Seurat 'FindAllMarkers'. Cluster identities were assigned based on known marker genes, including *Dmrt1*, *Stra8*, *Cenpa* and *Dazl* (spermatogonia); *Spo11*, *Piwil1*, *Tex101*, *Sycp3*, *Spata16* and *Ovol2* (spermatocytes); *Prm1*, *Prm2*, *Tnp1*, *Spata3* and *Txndc2* (elongating spermatids); *Sun5*, *Tex21*, *Tex36*, *Acrv1* and *Actl7b* (round spermatids); *Wt1*, *Cldn11* and *Amhr2* (Sertoli cells); *Insl3*, *Fabp3*, *Hsd3b1* and *Cyp11a1* (Leydig cells); *Cdh5*, *Pecam1* and *Vwf* (endothelial cells); *Lyz2*, *Mrc1* and *C1qc* (myeloid cells); *Lum*, *Dcn*, *Col1a1* and *Col1a2* (fibroblasts); and *Acta2* and *Myh11* (pericytes). Differential expression analysis between cells from control and *Brd8* cKO testes was performed using edgeR (v4.4.2), and genes with a false discovery rate (FDR) q-value<0.05 and $|\log_2$ fold change (FC)$|\geq 0.8$ were defined as significant. Gene ontology (GO) enrichment analysis was performed using clusterProfiler (v4.6.2) (Wu et al., 2021) with Benjamini–Hochberg correction. For pseudotime analysis, germ-cell populations were converted into Monocle3 objects (v1.3.7) (Cao et al., 2019). Cell–cell communication analysis was performed using the CellChat R package (v1.6.1) (Jin et al., 2021). Seurat objects containing annotated cell types were used as input. Gene expression data were normalized and processed following the standard CellChat workflow.

Statistical analysis

Unpaired, two-tailed t-test was used when two independent groups were compared. These statistical analyses were performed using R v4.4.3. $P<0.05$ was considered statistically significant.

Acknowledgements

We thank Dr Yumiko Saga (National Institute of Genetics, Japan) for providing Nanos3-Cre mice. We also thank Ms Meihui Zuo, Ms Dayeon Kim and Ms Hidemi Kasahara (The University of Tokyo) for their technical assistance, and Ms Tomoko Ando (Pathology Core laboratory, The University of Tokyo) for assistance in preparing the mouse tissue sections. The super-computing resource was provided by Human Genome Center, The Institute of Medical Science, The University of Tokyo (http://sc.hgc.jp/shirokane.html).

Competing interests

The authors declare no competing or financial interests.

Author contributions

Conceptualization: S.N., M.O., Y.F., K.Y.; Data curation: S.N.; Formal analysis: S.N., T.-W.W., E.S., K.Y.; Funding acquisition: S.N., K.Y.; Investigation: S.N., M.O., T.I., Y.I., K.Y.; Methodology: S.N., M.O.; Supervision: M.O., M.N., S.I., Y.F., K.Y.; Visualization: S.N., T.-W.W., K.Y.; Writing – original draft: S.N., K.Y.; Writing – review & editing: S.N., M.O., T.-W.W., T.I., Y.I., E.S., M.N., S.I., Y.F., K.Y.

Funding

This work was supported by Japan Society for the Promotion of Science KAKENHI grants [JP24K02318, JP22H04922 (AdAMS), and JP22H04923 (CoBiA) to K.Y.] and a Sasakawa Scientific Research Grant from the Japan Science Society (2023-4040 to S.N.). Open Access funding provided by the University of Tokyo. Deposited in PMC for immediate release.

Data and resource availability

The data generated in this study have been deposited in Gene Expression Omnibus under accession number GSE327037. All other relevant data and details of resources can be found within the article and its supplementary information.

First Person

This article has an associated First Person interview with the first author of the paper.

Peer review history

The peer review history is available online at https://journals.biologists.com/jcs/lookup/doi/10.1242/jcs.265013.reviewer-comments.pdf

References

Bhang, D. H., Kim, B.-J., Kim, B. G., Schadler, K., Baek, K.-H., Kim, Y. H., Hsiaos, W., Ding, B.-S., Rafii, S., Weiss, M. J. et al. (2018). Testicular endothelial cells are a critical population in the germline stem cell niche. *Nat. Commun.* **9**, 4379. doi:10.1038/s41467-018-06881-z

Busada, J., Niedenberger, B., Velte, E., Keiper, B. and Geyer, C. (2015). Mammalian target of rapamycin complex 1 (mTORC1) Is required for mouse spermatogonial differentiation in vivo. *Dev. Biol.* **407**, 90-102. doi:10.1016/j.ydbio.2015.08.004

Cai, Y., Jin, J., Tomomori-Sato, C., Sato, S., Sorokina, I., Parmely, T., Conaway, R. and Conaway, J. (2003). Identification of new subunits of the multiprotein mammalian TRRAP/TIP60-containing histone acetyltransferase complex. *J. Biol. Chem.* **278**, 42733-42736. doi:10.1074/jbc.C300389200

Cao, J., Spielmann, M., Qiu, X., Huang, X., Ibrahim, D., Hill, A., Zhang, F., Mundlos, S., Christiansen, L., Steemers, F. et al. (2019). The single-cell transcriptional landscape of mammalian organogenesis. *Nature* **566**, 496. doi:10.1038/s41586-019-0969-x

Cotto, K., Feng, Y., Ramu, A., Richters, M., Freshour, S., Skidmore, Z., Xia, H., McMichael, J., Kunisaki, J., Campbell, K. et al. (2023). Integrated analysis of genomic and transcriptomic data for the discovery of splice-associated variants in cancer. *Nat. Commun.* **14**, 1589. doi:10.1038/s41467-023-37266-6

Dobin, A., Davis, C., Schlesinger, F., Drenkow, J., Zaleski, C., Jha, S., Batut, P., Chaisson, M. and Gingeras, T. (2013). STAR: ultrafast universal RNA-seq aligner. *Bioinformatics* **29**, 15-21. doi:10.1093/bioinformatics/bts635

Fang, Q., Liu, B., Cen, J., Li, T., Ji, S., Li, W., Lu, G., Chen, Z., Wang, X., Bao, J. et al. (2025). PPP6R3-mediated dephosphorylation regulates mRNA translation during spermatogonial differentiation. *Commun. Biol.* **8**, 1114. doi:10.1038/s42003-025-08539-1

Filippakopoulos, P. and Knapp, S. (2014). Targeting bromodomains: epigenetic readers of lysine acetylation. *Nat. Rev. Drug Discov.* **13**, 337-356. doi:10.1038/nrd4286

Fujisawa, T. and Filippakopoulos, P. (2017). Functions of bromodomain-containing proteins and their roles in homeostasis and cancer. *Nat. Rev. Mol. Cell Biol.* **18**, 246-262. doi:10.1038/nrm.2016.143

Gewiss, R., Law, N., Helsel, A., Shelden, E. and Griswold, M. (2021). Two distinct Sertoli cell states are regulated via germ cell crosstalk. *Biol. Reprod.* **105**, 1591-1602. doi:10.1093/biolre/ioab160

Gilan, O., Rioja, I., Knezevic, K., Bell, M., Yeung, M., Harker, N., Lam, E., Chung, C., Bamborough, P., Petretich, M. et al. (2020). Selective targeting of BD1 and BD2 of the BET proteins in cancer and immunoinflammation. *Science* **368**, 387-394. doi:10.1126/science.aaz8455

Govin, J., Caron, C., Lestrat, C., Rousseaux, S. and Khochbin, S. (2004). The role of histones in chromatin remodelling during mammalian spermiogenesis. *Eur. J. Biochem.* **271**, 3459-3469. doi:10.1111/j.1432-1033.2004.04266.x

Hao, Y., Stuart, T., Kowalski, M., Choudhary, S., Hoffman, P., Hartman, A., Srivastava, A., Molla, G., Madad, S., Fernandez-Granda, C. et al. (2024). Dictionary learning for integrative, multimodal and scalable single-cell analysis. *Nat. Biotechnol.* **42**, 293-304. doi:10.1038/s41587-023-01767-y

Inoue, H., Sakurai, T., Hasegawa, K., Suzuki, A. and Saga, Y. (2022). NANOS3 suppresses premature spermatogonial differentiation to expand progenitors and fine-tunes spermatogenesis in mice. *Biol. Open* **11**, bio059146. doi:10.1242/bio.059146

Jin, S., Guerrero-Juarez, C., Zhang, L., Chang, I., Ramos, R., Kuan, C., Myung, P., Plikus, M. and Nie, Q. (2021). Inference and analysis of cell-cell communication using CellChat. *Nat. Commun.* **12**, 1088. doi:10.1038/s41467-021-21246-9

Kent, W., Zweig, A., Barber, G., Hinrichs, A. and Karolchik, D. (2010). BigWig and BigBed: enabling browsing of large distributed datasets. *Bioinformatics* **26**, 2204-2207. doi:10.1093/bioinformatics/btq351

Li, H. (2018). Minimap2: pairwise alignment for nucleotide sequences. *Bioinformatics* **34**, 3094-3100. doi:10.1093/bioinformatics/bty191

Li, H., Handsaker, B., Wysoker, A., Fennell, T., Ruan, J., Homer, N., Marth, G., Abecasis, G., Durbin, R. and Proc, G. P. D. (2009). The sequence alignment/map format and SAMtools. *Bioinformatics* **25**, 2078-2079. doi:10.1093/bioinformatics/btp352

Li, W., Wu, J., Kim, S., Zhao, M., Hearn, S., Zhang, M., Meistrich, M. and Mills, A. (2014). Chd5 orchestrates chromatin remodelling during sperm development. *Nat. Commun.* **5**, 3812. doi:10.1038/ncomms4812

Matzuk, M., McKeown, M., Filippakopoulos, P., Li, Q., Ma, L., Agno, J., Lemieux, M., Picaud, S., Yu, R., Qi, J. et al. (2012). Small-molecule inhibition of BRDT for male contraception. *Cell* **150**, 673-684. doi:10.1016/j.cell.2012.06.045

Miller, T., Simon, B., Rybin, V., Grötsch, H., Curtet, S., Khochbin, S., Carlomagno, T. and Müller, C. (2016). A bromodomain-DNA interaction facilitates acetylation-dependent bivalent nucleosome recognition by the BET protein BRDT. *Nat. Commun.* **7**, 13855. doi:10.1038/ncomms13855

Monden, T., Wondisford, F. and Hollenberg, A. (1997). Isolation and characterization of a novel ligand-dependent thyroid hormone receptor-coactivating protein. *J. Biol. Chem.* **272**, 29834-29841. doi:10.1074/jbc.272.47.29834

Nielsen, M., Petersen, C., Gliemann, J. and Madsen, P. (1996). Cloning and sequencing of a human cDNA encoding a putative transcription factor containing a bromodomain. *Biochim. Biophys. Acta Gene Struct. Expr.* **1306**, 14-16. doi:10.1016/0167-4781(95)00239-1

Ozawa, M., Taguchi, J., Katsuma, K., Ishikawa-Yamauchi, Y., Kikuchi, M., Sakamoto, R., Yamada, Y. and Ikawa, M. (2022). Efficient simultaneous double DNA knock-in in murine embryonic stem cells by CRISPR/Cas9 ribonucleoprotein-mediated circular plasmid targeting for generating gene-manipulated mice. *Sci. Rep.* **12**, 21558. doi:10.1038/s41598-022-26107-z

Quinlan, A. and Hall, I. (2010). BEDTools: a flexible suite of utilities for comparing genomic features. *Bioinformatics* **26**, 841-842. doi:10.1093/bioinformatics/btq033

Shang, E., Nickerson, H., Wen, D., Wang, X. and Wolgemuth, D. (2007). The first bromodomain of Brdt, a testis-specific member of the BET sub-family of double-bromodomain-containing proteins, is essential for male germ cell differentiation. *Development* **134**, 3507-3515. doi:10.1242/dev.004481

Sun, F., Palmer, K. and Handel, M. (2010). Mutation of Eif4g3, encoding a eukaryotic translation initiation factor, causes male infertility and meiotic arrest of mouse spermatocytes. *Development* **137**, 1699-1707. doi:10.1242/dev.043125

Sun, X., Klingbeil, O., Lu, B., Wu, C., Ballon, C., Ouyang, M., Wu, X., Jin, Y., Hwangbo, Y., Huang, Y. et al. (2023). BRD8 maintains glioblastoma by epigenetic reprogramming of the p53 network. *Nature* **613**, 195-202. doi:10.1038/s41586-022-05551-x

Suzuki, H., Tsuda, M., Kiso, M. and Saga, Y. (2008). Nanos3 maintains the germ cell lineage in the mouse by suppressing both Bax-dependent and -independent apoptotic pathways. *Dev. Biol.* **318**, 133-142. doi:10.1016/j.ydbio.2008.03.020

Tanaka, T., Hosokawa, M., Vagin, V., Reuter, M., Hayashi, E., Mochizuki, A., Kitamura, K., Yamanaka, H., Kondoh, G., Okawa, K. et al. (2011). Tudor domain containing 7 (Tdrd7) is essential for dynamic ribonucleoprotein (RNP) remodeling of chromatoid bodies during spermatogenesis. *Proc. Natl. Acad. Sci. USA* **108**, 10579-10584. doi:10.1073/pnas.1015447108

Tang, A., Soulette, C., van Baren, M., Hart, K., Hrabeta-Robinson, E., Wu, C. and Brooks, A. (2020). Full-length transcript characterization of SF3B1 mutation in chronic lymphocytic leukemia reveals downregulation of retained introns. *Nat. Commun.* **11**, 1438. doi:10.1038/s41467-020-15171-6

Thorvaldsdóttir, H., Robinson, J. and Mesirov, J. (2013). Integrative Genomics Viewer (IGV): high-performance genomics data visualization and exploration. *Brief. Bioinform.* **14**, 178-192. doi:10.1093/bib/bbs017

Wang, X., Sang, M., Gong, S., Chen, Z., Zhao, X., Wang, G., Li, Z., Huang, Y., Chen, S., Xie, G. et al. (2022). BET bromodomain inhibitor JQ1 regulates spermatid development by changing chromatin conformation in mouse spermatogenesis. *Genes Dis.* **9**, 1062-1073. doi:10.1016/j.gendis.2020.12.012

Wu, T., Hu, E., Xu, S., Chen, M., Guo, P., Dai, Z., Feng, T., Zhou, L., Tang, W., Zhan, L. et al. (2021). clusterProfiler 4.0: A universal enrichment tool for interpreting omics data. *Innovation* **2**, 100141. doi:10.1016/j.xinn.2021.100141

Yamaguchi, K., Sakai, M., Shimokawa, T., Yamada, Y., Nakamura, Y. and Furukawa, Y. (2010). C20orf20 (MRG-binding protein) as a potential therapeutic target for colorectal cancer. *Br. J. Cancer* **102**, 325-331. doi:10.1038/sj.bjc.6605500

Yamaguchi, K., Nakagawa, S., Saku, A., Isobe, Y., Yamaguchi, R., Sheridan, P., Takane, K., Ikenoue, T., Zhu, C., Miura, M. et al. (2023). Bromodomain protein BRD8 regulates cell cycle progression in colorectal cancer cells through a TIP60-independent regulation of the pre-RC complex. *iScience* **26**, 106563. doi:10.1016/j.isci.2023.106563

Yamaguchi, K., Nakagawa, S. and Furukawa, Y. (2024). Understanding the role of BRD8 in human carcinogenesis. *Cancer Sci.* **115**, 2862-2870. doi:10.1111/cas.16263

Yang, S., Corbett, S., Koga, Y., Wang, Z., Johnson, W., Yajima, M. and Campbell, J. (2020). Decontamination of ambient RNA in single-cell RNA-seq with DecontX. *Genome Biol.* **21**, 57. doi:10.1186/s13059-020-1950-6

Yu, X., He, T., Tong, Z., Liao, L., Huang, S., Fakhouri, W., Edwards, D. and Xu, J. (2023). Molecular mechanisms of TWIST1-regulated transcription in EMT and cancer metastasis. *EMBO Rep.* **24**, e56902. doi:10.15252/embr.202356902

Yuan, L., Liu, J., Zhao, J., Brundell, E., Daneholt, B. and Höög, C. (2000). The murine SCP3 gene is required for synaptonemal complex assembly, chromosome synapsis, and male fertility. *Mol. Cell* **5**, 73-83. doi:10.1016/S1097-2765(00)80404-9

Zhou, Z., Kawabe, H., Suzuki, A., Shinmyozu, K. and Saga, Y. (2017). NEDD4 controls spermatogonial stem cell homeostasis and stress response by regulating messenger ribonucleoprotein complexes. *Nat. Commun.* **8**, 15662. doi:10.1038/ncomms15662